Protonation of β-Cyanoenamines: NMR Spectroscopic and Calculational Studies of Ketenimine Amidinium Ion Formation

Tammy J. Dwyer,*,† Paul G. Jasien,‡ Scott M. Kirkowski,† Charles M. Buxton,† Jeannie M. Arruda,† and Gregory W. Mitchell†

Contribution from the Department of Chemistry, University of San Diego, 5998 Alcala Park, San Diego, California 92110, and Department of Chemistry, California State University, San Marcos, San Marcos, California 92096

Received August 21, 1998. Revised Manuscript Received October 21, 1998

Abstract: NMR spectroscopy and quantum mechanical calculations have been used to investigate the protonation of β-cyanoenamines. One-dimensional variable-temperature spectroscopy, two-dimensional exchange spectroscopy (2D EXSY), and density functional calculations provide convincing evidence that the favored site of protonation in 1,1-bis(dimethylamino)-2-cyano-2-*p*-X-phenyl-substituted ethylenes (X = NO_2, CF_3, Br, F, or CH_3) is the nitrogen of the cyano group. This results in the formation of a ketenimine amidinium ion in solution. When X is less electron withdrawing than $-NO_2$, an equilibrium mixture is formed consisting of 60−93% CN-protonated enamine with the remainder protonated at the β-carbon. Calculational results also support predominantly CN-protonation in these systems. Both experimental and calculational results show no evidence of protonation at the amino nitrogen.

Introduction

The electronic structures and reactivities of push−pull enamines have long been subjects of chemical interest, posing unique challenges with regard to their study.[1−4] A push−pull enamine is defined by one or more electron donor groups (typically $-NR_2$ groups) situated on one carbon of a C=C and one or more acceptor groups (such as $-NO_2$, −CN, or −C(=O)R) at the other carbon. Such an arrangement leads to a highly delocalized π electron system and polarization of the C=C. These systems demonstrate interesting dynamic behavior as well, such as facile rotations about the C=C and hindered rotations about the C−N bonds.[5−7] The push−pull effect leads to a substantially lower C=C rotational barrier (10−25 kcal mol^{-1}) relative to ethylene (65 kcal mol^{-1}) and an increased C−N barrier (8−17 kcal mol^{-1}) compared to a nonconjugated amino group. These low C=C barriers and high C−N barriers have been explained in terms of the capacity of the donor and acceptor groups to stabilize the developing dipolar transition state for rotation.

The structure and reactivity of a push−pull enamine are intimately linked. Both are influenced by the amino group substituents and the nature of the electron-withdrawing groups. Structurally, steric interactions between electron donor and acceptor groups lead to a nonplanar or twisted carbon−carbon double bond. The degree of nonplanarity directly effects the extent of conjugation between the lone-pair electrons of the amino nitrogen and the carbon−carbon double bond. Consequently, delocalization of electron density onto the β-carbon atom (and the electron acceptor groups) is diminished as is the reactivity at these sites. As one might expect, the effect is magnified in 1,1-enediamines in which a twist angle about the C=C can be as large as 85°.[8] These systems tend to show decreased reactivity relative to the parent enamine.

Although a systematic study of the reactivity of enamines as a function of electron-accepting groups has not been done, the reactions of enamines with electrophiles has been well documented.[9−12] A reaction of particular interest is the first step of enamine hydrolysis, namely, reaction of an enamine with the simplest electrophile, a hydrogen ion. Enamines exhibit atypical acid−base properties relative to simple amines. The basic nature of enamines derives from a mesomeric effect that leads to two possible sites of protonation. Protonation at the nucleophilic β-carbon of an enamine results in the iminium ion

† University of San Diego.
‡ California State University.

(1) (a) Osman, R.; Zunger, A.; Shvo, Y. *Tetrahedron* **1978**, *34*, 2315. (b) Olsson, T.; Sandstrøm, J. *Acta Chem. Scand. Ser. B* **1982**, 23. (c) Favini, G.; Gamba, A.; Todeschini, R. *J. Chem. Soc., Perkin Trans. 2* **1985**, 915.

(2) Pappalardo, R. R.; Marcos, E. S.; Ruiz-Lopez, M. F.; Rinaldi, D.; Rivail, J.-L. *J. Phys. Org. Chem.* **1991**, *4*, 141. Pappalardo, R. R.; Marcos, E. S.; Ruiz-Lopez, M. F.; Rinaldi, D.; Rivail, J.-L. *J. Am. Chem. Soc.* **1993**, *115*, 3722.

(3) Wong, M. W.; Frisch, M. J.; Wiberg, K. B. *J. Am. Chem. Soc.* **1991**, *113*, 4776. Head-Gordon, M.; Pople, J. A. *J. Phys. Chem.* **1993**, *97*, 1147.

(4) Dwyer, T. J.; Jasien, P. G. *J. Mol. Struct. (THEOCHEM)* **1996**, *363*, 139.

(5) (a) Lister, D. G.; Macdonald, J. N.; Owen, N. L. *Internal Rotation and Inversion* Academic: London, 1978; references cited therein. (b) Sandstrøm, J. *Top. Stereochem.* **1983**, *14*, 84 and references cited therein.

(6) Shvo, Y.; Shanan-Atidi, H. *J. Am. Chem. Soc.* **1969**, *91*, 6683. Shvo, Y.; Shanan-Atidi, H. *J. Am. Chem. Soc.* **1969**, *91*, 6689. Dahlqvist, K. *Acta Chem. Scand.* **1970**, *24*, 1941. Wennerbeck, I.; Sandstrøm, J. *Org. Magn. Reson.* **1972**, *4*, 783.

(7) Kessler, H. *Chem. Ber.* **1970**, *103*, 973.

(8) Baum, K.; Bigelow, S. S.; Nauyen, N. V.; Archibald, T. G.; Gilardi, R.; Flippen-Anderson, J. L.; George, C. *J. Org. Chem.* **1992**, *57*, 235.

(9) Stork, G.; Terrel, R.; Scmuszkovicz, J. *J. Am. Chem. Soc.* **1954**, *76*, 2029. Stork, G.; Landesman, H. *J. Am. Chem. Soc.* **1956**, *78*, 5128, 5129.

(10) Elkik, E. *Bull Soc. Chim. Fr.* **1960**, 972. Kuehne, M. E.; Garbacik, T. *J. Org. Chem.* **1970**, *35*, 1555. Capon, B.; Wu, Z.-P. *J. Org. Chem.* **1990**, *55*, 5, 2317. Hickmott, P. W. In *The Chemistry of Enamines Part 1*; Rappoport, Z., Ed.; John Wiley & Sons: New York, 1994; p 727, references cited therein.

(11) Hickmott, P. W. *Tetrahedron* **1982**, *38*, 1975.

(12) Catalan, J.; Blanco, F. G. In *The Chemistry of Enamines Part 1*; Rappoprt, Z., Ed.; John Wiley & Sons: New York, 1994; p 695, and references cited therein.

10.1021/ja983016m CCC: $15.00
Published on Web 11/25/1998

(**1**) while protonation at the amine nitrogen leads to the enammonium ion (**2**).

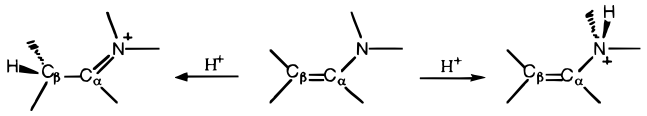

1 **2**

Ordinarily, the amino nitrogen or the β-carbon of an enamine has been considered as a likely site of protonation in hydrolysis reactions. Coward and Bruice[13] have studied the mechanism of hydrolysis of several β-cyanoenamines, which typically follow first-order kinetics with general acid catalysis, and have observed anomalous behavior below pH 1. They attribute this result to a change in mechanism from rate-determining general acid-catalyzed tautomerism between the enamine and the C_β-protonated enamine to rate-determining hydrolysis of the C_β-protonated enamine. However, Kresge's review[14] of the literature of hydrolysis of enamines points out that protonation of the cyano nitrogen (with formation of the ketenimine) cannot be ruled out as an explanation of the observed behavior at pH < 1 in Bruice's work. Few reports of the formation of unsubstituted ketenimines may be found. Fleury and Libis[15a] reported the formation of crystalline solid ketenimines upon treatment of acylmalononitriles with acid. Ferris and Trimmer[15b] reported the detection by IR of the transient ketenimine of several primary enaminonitriles following UV irradiation at −196 °C, though the attributed stretching frequency disappeared at higher temperatures.

How does the push−pull effect alter the basicity of an enamine? In this study, we have investigated 1,1-bis(dimethylamino)-2-cyano-2-*p*-X-phenyl-substituted ethylenes **3**−**7** under acidic conditions. Our aim in this report is to provide compelling evidence for ketenimine formation via protonation of a cyano nitrogen through experimental NMR data and quantum mechanical calculations.

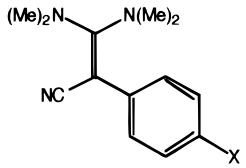

3 X = NO_2
4 X = CF_3
5 X = Br
6 X = F
7 X = CH_3

Experimental Section

Materials. Reagents and solvents were purchased from Aldrich. The solvents were purified according to accepted procedures.[16]

Synthesis of Enamines. General Procedure. The enamines **3**−**7** were prepared according to Scheme 1 where X = NO_2, CF_3, Br, F, or CH_3.

The chloroformamidinium chloride **8** was prepared from tetramethylurea and oxalyl chloride as previously described.[17] In a typical experiment, oxalyl chloride (0.01 mol, 25 g) was dissolved in 40 mL CH_2Cl_2 under an inert atmosphere and added to tetramethylurea (0.13 mol, 15.5 g) dissolved in 25 mL CH_2Cl_2 and stirred. The solution turned lime green with the evolution of gas. Solid **8** was precipitated from solution by the addition of 30 mL of diethyl ether. The solvent was

Scheme 1

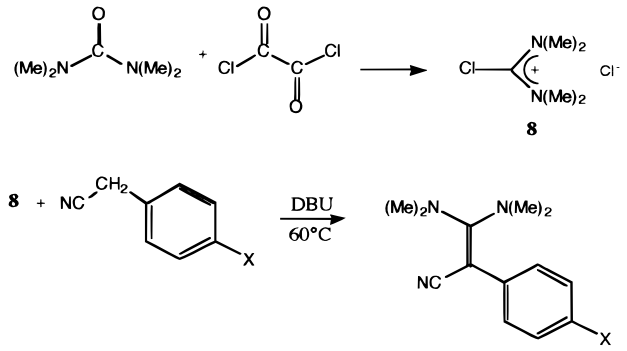

decanted, and the solid washed four times with diethyl ether and finally dried under a stream of nitrogen gas. The enamines were prepared according to the method of Kessler.[7] Chloroformamidinium chloride (**8**, 0.01 mol, 1.7 g) in 5 mL of CH_3CN was added to 0.01 mol of the substituted phenylacetonitrile dissolved in 15 mL of CH_2Cl_2 plus 2.5 equiv (0.025 mol, 3.75 mL) of 1,8-diazabicyclo[5.4.0]undec-7-ene (DBU). The reaction mixture was refluxed for 12 h and cooled to room temperature, and the solvents were evaporated. The residue was dissolved in a small amount of CH_2Cl_2 and then purified by column chromatography on silica gel using CH_2Cl_2 as solvent. For **3**: mp 142−144 °C; ^{1}H NMR ($CDCl_3$) δ 2.78 (6H, br s), 3.05 (6H, br s), 6.95 (2H, d), 8.05 (2H, d). For **4**: mp 95−97 °C; ^{1}H NMR ($CDCl_3$) δ 2.70 (6H, s), 3.05 (6H, br s), 7.09 (2H, d), 7.49 (2H, d). For **5**: mp 127−128 °C; ^{1}H NMR ($CDCl_3$) δ 2.65 (6H, s), 3.00 (6H, br s), 6.87 (2H, d), 7.35 (2H, d). For **6**: mp 65−68 °C; ^{1}H NMR ($CDCl_3$) δ 2.53 (6H, s), 2.91 (6H, br s), 6.90 (4H, m). For **7**: mp 61−64 °C; ^{1}H NMR ($CDCl_3$) δ 2.20 (3H, s), 2.52 (6H, br s), 2.89 (6H, br s), 6.83 (2H, d), 6.97 (2H, d).

NMR Methods. Proton NMR spectra were acquired on a Varian UNITY-300 spectrometer. Samples were prepared by dissolving 10 mg of the enamine in 700 μL of deuterated solvent ($CDCl_3$, CD_2Cl_2, or $CD_3C(O)CD_3$). Aliquots of 0.25−1.5 equiv of trifluoroacetic acid (TFA) were then added to the sample. The 1D variable-temperature spectra were regulated to ±0.1 °C. All 2D exchange spectroscopy (EXSY)[18] data were acquired at 300 MHz using a NOESY sequence with the States et al.[19] phase-cycling method to generate pure absorption phase spectra. The spectra were collected with 1024 points in t_2 using a spectral width of 2800 Hz and a mixing time of 350 ms. Typically 256 t_1 experiments were recorded and zero-filled to 1K. For each t_1 value 8 scans were signal averaged using a recycle delay of 4 s.

Computational Methods. All calculations were performed with the Gaussian 94 program package[20] on an IBM RISC/6000 workstation. Calculations used the density functional method denoted B3LYP[21] which includes nonlocal corrections to the correlation functional. The inclusion of electron correlation was deemed important in accurately describing these systems. Further, density functional methods offer less computationally demanding alternatives to Møller−Plesset second-order perturbation theory (MP2)[22] calculations with essentially the same

(13) Coward, J. K.; Bruice, T. C. *J. Am. Chem. Soc.* **1969**, *91*, 5329.
(14) Keeffe, J. R.; Kresge, A. J. In *The Chemistry of Enamines Part 2*; Rappoport, Z., Ed.; John Wiley & Sons: New York, 1994; p 1049.
(15) (a) Fleury, J.-P.; Libis, B. *Compt. Rend.* **1963**, *256*, 2419. (b) Ferris, J. P.; Trimmer, R. W. *J. Org. Chem.* **1976**, *41*, 19.
(16) Gordon, A. J.; Ford, R. A. *The Chemist's Companion*; John Wiley & Sons: New York, 1972.
(17) Eilingsfeld, H.; Neubauer, G.; Seefelder, M.; Weidinger, H. *Chem. Ber.* **1964**, *97*, 1232.
(18) Perrin, C. L.; Gipe, R. K. *J. Am. Chem. Soc.* **1984**, *106*, 4036. Perrin, C. L.; Dwyer, T. J. *Chem. Rev.* **1990**, *90*, 935.
(19) States, D. J.; Haberkorn, R. A.; Ruben, D. J. *J. Magn. Reson.* **1982**, *48*, 286.
(20) Gaussian 94, Revision B.1; Frisch, M. J.; Trucks, G. W.; Schlegel, H. B.; Gill, P. M. W.; Johnson, B. G.; Robb, M. A.; Cheeseman, J. R.; Keith, T.; Petersson, G. A.; Montgomery, J. A.; Raghavachari, K.; Al-Laham, M. A.; Zakrzewski, V. G.; Ortiz, J. V.; Foresman, J. B.; Cioslowski, J.; Stefanov, B. B.; Nanayakkara, A.; Challacombe, M.; Peng, C. Y.; Ayala, P. Y.; Chen, W.; Wong, M. W.; Andres, J. L.; Replogle, E. S.; Gomperts, R.; Martin, R. L.; Fox, D. J.; Defrees, D. J.; Baker, J.; Stewart, J. J. P.; Head-Gordon, M.; Gonzalez, C.; Pople, J. A. Gaussian, Inc., Pittsburgh, PA, 1995.
(21) (a) Lee, C.; Yang, W.; Parr, R. G. *Phys. Rev. B* **1988**, *37*, 785. (b) Becke, A. D. *Phys. Rev. A* **1988**, *38*, 3098. (c) Becke, A. D. *J. Chem. Phys.* **1993**, *98*, 5648.
(22) Møller, C.; Plesset, M. S. *Phys. Rev.* **1934**, *46*, 618.

Scheme 2

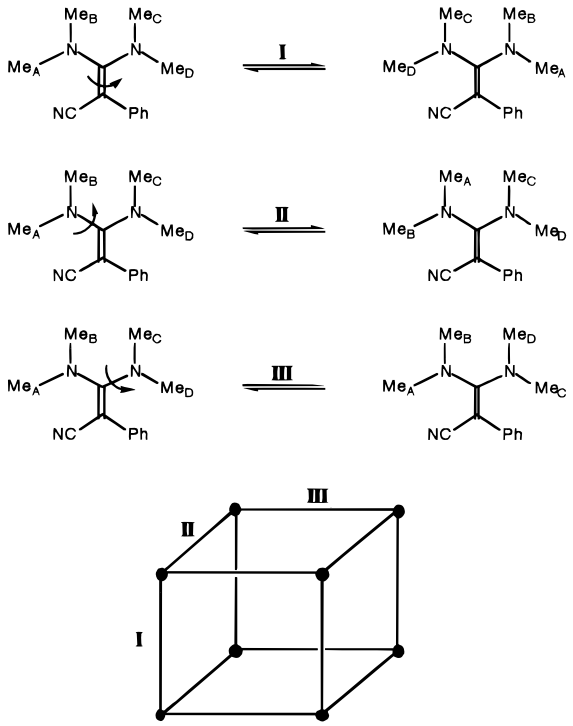

accuracy.[23] Another advantage of the density functional methods, in this particular case, was the stability of the wave function. We have found that the restricted Hartree−Fock (RHF) method for these closed shell systems has an RHF → UHF (unrestricted Hartree−Fock) instability.[24,25] This instability would lead to complications, such as spin contamination, if UHF and UMP2 wave functions were used in these calculations.

The basis sets used included the standard 6-31G set and a modified 6-31G* set that added p-polarization functions only on the H^+. We denote this 6-31G*+p. An extended 6-311G(2d,p) basis set was used in selected calculations. Geometries were optimized with both the 6-31G and 6-31G*+p sets. Structures were converged without any symmetry constraints and achieved convergence to 0.001 Å in bond lengths and 0.1° in most bond angles. In a few cases, some torsional angles with very flat potentials had convergence to slightly greater values, however, the associated energy changes were less than 1.0×10^{-8} a.u. Analytic second derivatives were calculated for the CN- and C_β-protonated forms with the 6-31G basis set in order to assess the effect of zero-point energy (ZPE) corrections on the relative stability.

Results

NMR Spectroscopic Analyses. The dynamic processes occurring in enamines **3**−**7** are diagrammed in Scheme 2. There are three rotational processes that serve to interconvert the eight conformers (denoted as filled circles at the corners of the cube in Scheme 2).

Rotation about the C═C bond (process I, vertical lines in Scheme 2) leads to interchange of the *N*,*N*-dimethyl groups. Rotations about C−N bonds (processes II and III in Scheme 2) lead to exchange of the *N*-methyl environments on an amino group. It was immediately obvious that the addition of TFA to samples containing **3**−**7** in any deuterated solvent affected the C═C and/or C−N bond rotational barriers. This was indicated by the dramatic changes in the peak patterns in the *N*-methyl regions of the ^{1}H NMR spectra. For brevity, we discuss the spectra of compounds **3**, **6**, and **7** in the presence of 1.5 equiv of TFA, since the spectral characteristics do not change above 1.0 equiv of acid. Figure 1 (bottom trace) shows the proton spectrum of **3** in $CDCl_3$ at 23 °C in the absence of acid (unprotonated). The broad peaks at 3.0 ppm arise from the *N*-methyl protons (Scheme 2, A, B, C, and D) in **3**, and those at 7.0 and 8.1 ppm are due to the *p*-nitrophenyl aromatic protons. At room temperature, C═C rotation occurs at a moderate rate while C−N bond rotations are fast on the NMR time scale. As the temperature is decreased (not shown), the C═C rotation is nearly stopped while the C−N rotations are slowed, distinguishing all four *N*-methyl group proton environments. Figure 1 also shows the NMR spectrum of **3** in $CDCl_3$ at 23 °C plus 1.5 equiv of TFA. Clearly, the *N*-methyl signals are coalesced relative to those in unprotonated **3** which indicates a faster exchange rate.

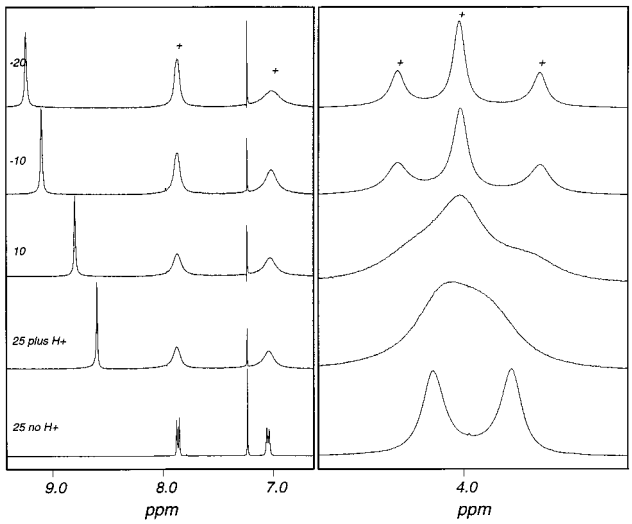

Figure 1. NMR data showing unprotonated **3** (bottom trace) and the variable-temperature spectra of **3** in $CDCl_3$ with 1.5 equiv of TFA added. The plus signs indicate the aromatic (downfield) and *N*-methyl (upfield) resonances of the ketenimine amidinium ion **9** with X = NO_2.

The effect of decreasing temperature on the NMR spectrum of **3** plus 1.5 equiv of TFA in $CDCl_3$ solution is displayed in Figure 1. As the temperature is decreased, the *N*-methyl groups become distinguishable. The peak assignments for the *N*-methyl proton signals in **3** at −20 °C are (using amidine nomenclature) *exo*-N−CH_3 (δ3.2, cis to cyano group), *endo*-N−CH_3 (δ3.0, cis to cyano group), *endo*-N−CH_3 (δ3.0, trans to cyano group), and *exo*-N−CH_3 (δ2.7, trans to cyano group).[7] The *endo*-N−CH_3 signals are overlapped leading to only three peaks in this region for **3**. The signals at 7.0 and 8.1 ppm are due to the *p*-nitrophenyl ring protons, while the peak at approximately 9 ppm is due to excess TFA. The *N*-methyl proton region of the 2D EXSY spectrum of **3** at −20 °C is shown in Figure 2. Using Scheme 2 as a guide, (the rotational processes are the same, except now we have a protonated molecule) the diagonal of the EXSY gives the relative chemical shifts of the *N*-methyl proton signals assigned above. The cross-peaks labeled 1 and 1′ arise due to both C═C and C−N (cis to cyano group) rotational processes. Similarly, cross-peaks 3 and 3′ are due to C═C and C−N (trans to cyano group). The cross-peaks labeled 2 and 2′ arise strictly from C═C rotation.

We have also studied enamine **6** under acidic conditions in $CDCl_3$ plus 1.5 equiv of TFA. Figure 3 shows the variable-

(23) (a) Schmiedekamp, A. M.; Topol, I. A.; Burt, S. K.; Razafinjanahary, H.; Chermette, H.; Pfaltzgraff, T.; Michejda, C. J. *J. Comput. Chem.* **1994**, *15*, 975. (b) Martell, J. M.; Goddard, J. D.; Eriksson, L. A. *J. Phys. Chem. A* **1997**, *101*, 1927.

(24) (a) Seeger, R.; Pople, J. A. *J. Chem. Phys.* **1977**, *66*, 3045. (b) Schlegel, H. B.; McDouall, J. J. W. In *Computational Advances in Organic Chemistry: Molecular Structure and Reactivity*; Ogretir, Csizmadia, I. G., Eds.; NATO ASI Series, Series C: Mathematical and Physical Sciences; Kluwer: Dordrecht, The Netherlands, 1991; Vol. 330, p 167ff.

(25) Jasien, P. G. Unpublished results.

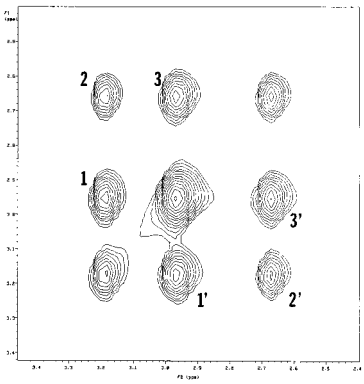

Figure 2. Expansion of the *N*-methyl region of the 2D EXSY spectrum of **3** in $CDCl_3$ plus 1.5 equiv of TFA. Cross-peak identities are described in the text.

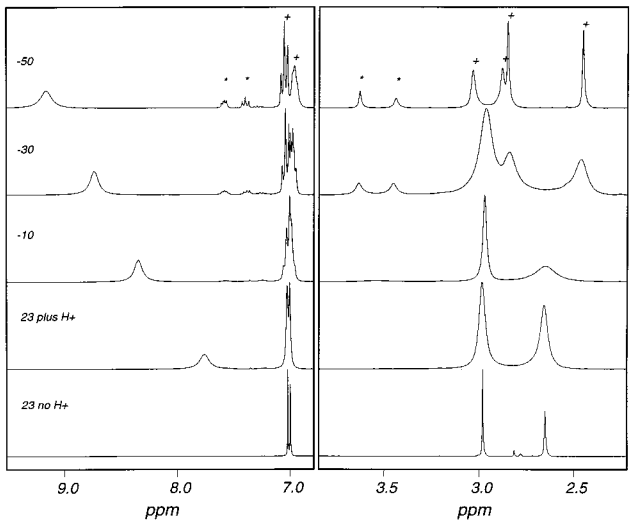

Figure 3. NMR data showing unprotonated **6** (bottom trace) and the variable-temperature spectra of **6** in $CD_3C(O)CD_3$ with 1.5 equiv of TFA added. The plus signs indicate the aromatic (downfield) and *N*-methyl (upfield) resonances of the ketenimine amidinium ion **9** with X = F. The stars mark the aromatic (downfield) and *N*-methyl (upfield) resonances of the C_β-protonated amidinium ion **12** with X = F.

temperature NMR spectra associated with this compound. Unlike **3**, the *N*-methyl proton region in enamine **6** develops a six-peak pattern at low temperature (−30 to −50 °C). The peak assignments for the *N*-methyl proton region in protonated **6** are $N-(CH_3)_2$ (δ3.7, cis to cyano group) and $N-(CH_3)_2$ (δ3.5, trans to cyano group) of a C_β-protonated form of **6** and *exo*-$N-CH_3$ (δ3.1, cis to cyano group), *endo*-$N-CH_3$ (δ2.9, cis to cyano group), *endo*-$N-CH_3$ (δ2.85, trans to cyano group), and *exo*-$N-CH_3$ (δ2.5, trans to cyano group) of a CN-protonated form. The difference in line widths of the *N*-methyl peaks for C_β-protonated forms of **6** is a consequence of the difference in T_2 of the *exo*- and *endo*-$N-CH_3$ groups. The resulting 2D EXSY spectrum (Figure 4) acquired at −50 °C suggests the presence of two forms of protonated **6** which are in intermolecular exchange due to proton transfer and intramolecular exchange due to restricted rotational processes. Integration of the 1D spectrum at −50 °C yields a ratio of the two forms of 87 (CN-protonated):13 (C_β-protonated). Further evidence for two distinct forms of protonated **6** is provided in the aromatic region of the ^1H spectrum. In this region, two sets of signals are seen in a ratio of 13 (downfield signal):87 (upfield signal). Note that these two forms are in intermolecular exchange as revealed by the cross-peaks in the downfield (6.9−7.6 ppm) region of Figure 4.

Table 1. Energies (kcal mol^{-1}) of Protonated Species from B3LYP Calculations Relative to the CN−Protonated System[a−c]

system	basis set	Δ*E*(C)	Δ*E*(C) + ZPE	Δ*E*(N)
3	6-31G*+p	1.6	2.3	16.3
	6-311G(2d,p)	1.7	2.4	
4	6-31G*+p	1.0	1.8	16.0
	6-311G(2d,p)	1.2	2.0	
6	6-31G*+p	0.7	1.7	15.4
	6-311G(2d,p)	0.9	1.9	
7	6-31G*+p	0.4	1.4	15.2
	6-311G(2d,p)	0.5	1.5	

[a] 6-311G(2d,p) energies were evaluated at the 6-31G*+p-optimized geometries. [b] E(CN-protonated) = 0. Δ*E*(X) represents the energy relative to CN-protonated form. [c] ZPE-corrected results use B3LYP/6-31G calculated values.

Protonation of compound **7** under similar sample conditions as above yielded the variable-temperature spectra for the *N*-methyl proton region displayed in Figure 5. A similar peak pattern as in protonated **6** arises at still lower temperature (−60 °C), indicating two forms of protonated **7** in solution. In protonated **7**, the integration of the signals yields a ratio of 60:40 for the two forms.

Compounds **4** and **5** show protonation behavior intermediate between that of **3** and **6** (as would be expected since they contain substituents with σ values intermediate between those for $-NO_2$ and −F). Both protonated **4** and **5** show CN-protonated enamine to C_β-protonated enamine ratios of 93:7 in all solvents studied.

A Hammett-type free energy relationship for the C_β-protonated/CN-protonated equilibrium is presented in Figure 6. A good linear correlation with $\rho = +1.8$ is obtained. This moderately large positive ρ value implies that the β-carbon is extremely electron-deficient relative to the cyano nitrogen. Further, the distribution of the electron density in the molecules prior to protonation is modulated by the substituted phenyl ring.

Computations. Table 1 displays the calculated stabilities of the various protonated forms of **3**, **4**, **6**, and **7** for the B3LYP calculations with the 6-31G*+p and 6-311G(2d,p) basis sets. The calculated relative energies of the CN-protonated and C_β-protonated forms change by 0.2 kcal mol^{-1} or less on going from the 6-31G*+p to the 6-311(2d,2p) basis set. The results for the B3LYP/6-31G calculations are not shown since they are in very close agreement with the larger basis set calculations. For all four push−pull systems studied, the most favorable protonation site is the nitrogen of the cyano group, followed closely by C_β, and then the amino nitrogen. The calculated ZPE corrections favor the CN-protonated enamine over the C_β-protonated form by 0.7−1.0 kcal mol^{-1}.

The proton affinities (PAs) for the push−pull systems show an interesting trend. The results indicate that the larger the energy difference between the C_β-protonated and CN-protonated forms, the smaller the PAs. The PAs (kcal mol^{-1}) for the cyano nitrogen site based on ZPE corrected 6-31G*+p calculations are **3** (223.5), **4** (227.5), **6** (230.4), and **7** (233.3). The trend **3** < **4** < **6** < **7** holds, regardless of the site of protonation.

Table 2 lists selected calculated bond lengths and angles for the protonated and unprotonated push−pull systems studied in this work. For brevity, only average C−N (amine) bond lengths are listed. These bond lengths were generally within 0.005 Å, but differed by as much as 0.009 Å in one instance. In all cases, the geometry around the ethylenic carbon atoms is planar which is also true for the amino nitrogen atoms.

Lastly, Table 3 gives the calculated electric dipole moments for the unprotonated push−pull systems. In addition, qualitative information on the charge partitioning derived from a Mulliken population analysis is given. The results are listed for two

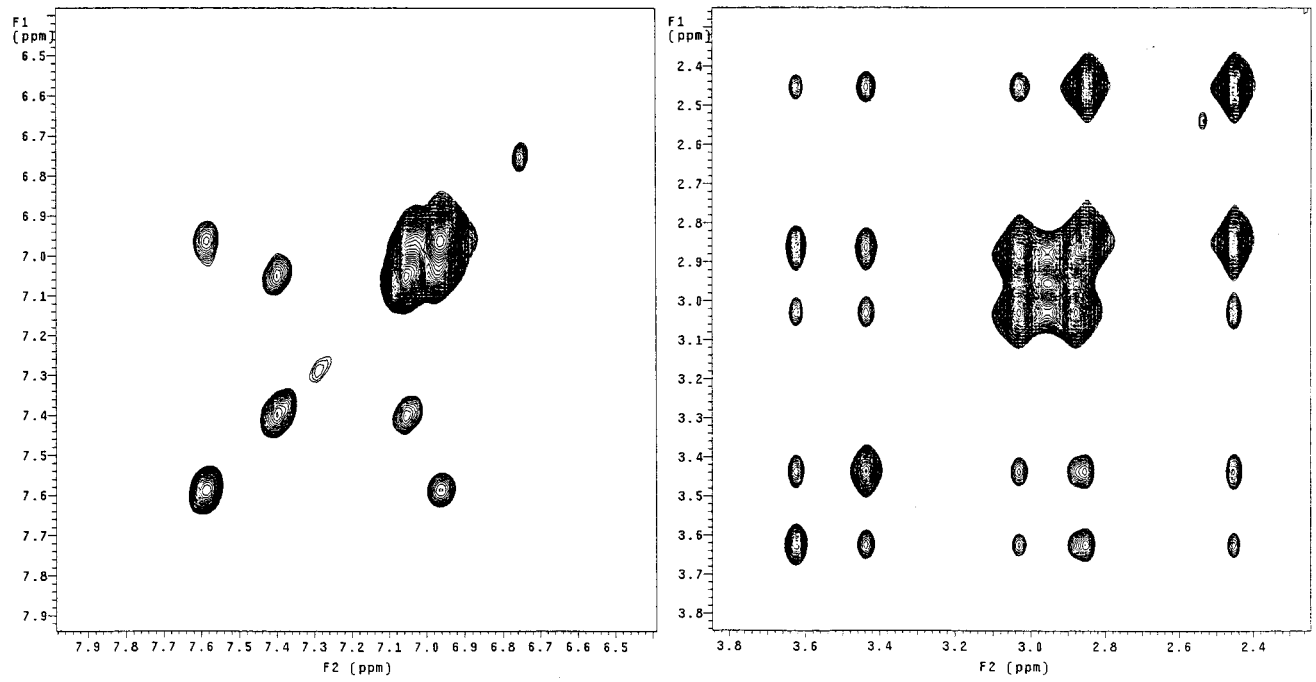

Figure 4. The 2D EXSY spectrum of **6** in $CD_3C(O)CD_3$ plus 1.5 equiv of TFA. The cross-peak patterns in the aromatic (downfield) and *N*-methyl (upfield) regions are described in the text.

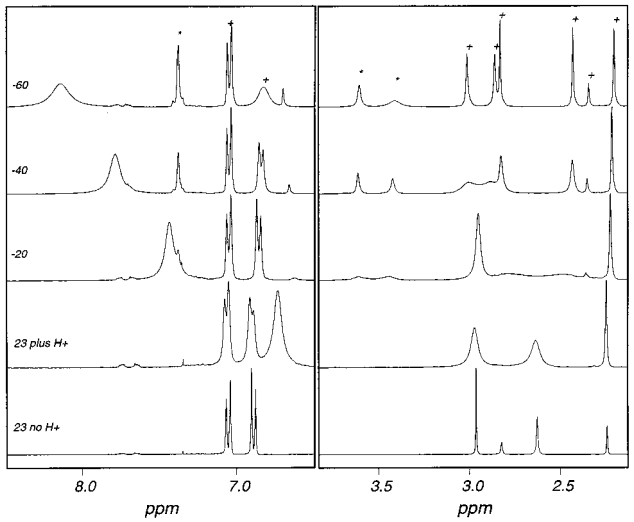

Figure 5. NMR data showing unprotonated **7** (bottom trace) and the variable-temperature spectra of **7** in $CD_3C(O)CD_3$ with 1.5 equiv of TFA added. The plus signs indicate the aromatic (downfield) and *N*-methyl (upfield) resonances of the ketenimine amidinium ion **9** with X = CH_3. The stars mark the aromatic (downfield) and *N*-methyl (upfield) resonances of the C_β-protonated amidinium ion **12** with X = CH_3.

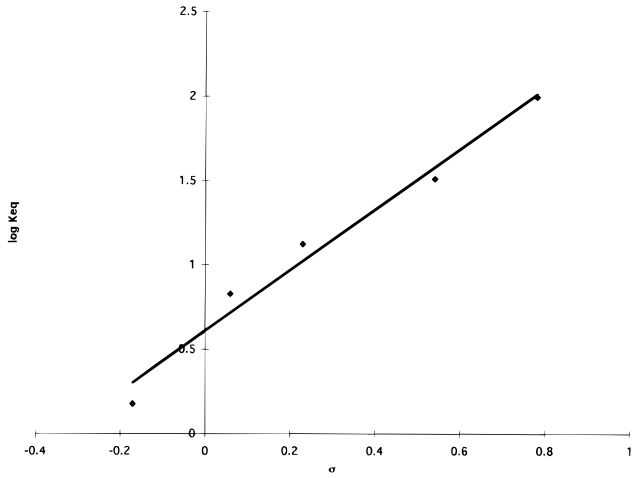

Figure 6. Hammett-type plot for the equilibrium C_β-protonated ⇌ CN-protonated.

separate partitionings. The first separates the molecule between the two ethylenic carbon atoms to obtain partial charges on the donor and acceptor subsystems. The second sums the charges only on the phenyl ring and phenyl ring substituents. Division of the molecule into large subsystems mitigates somewhat the problems associated with using Mulliken populations to assign partial charges.

Discussion

Protonation of **3** at either amino nitrogen is ruled out based on two lines of evidence. First, the NMR spectra are *inconsistent* with N-protonation, since N-protonation would give rise to rapid, unhindered rotation about the C−N single bonds; the observed slowing of C−N rotations at moderate temperatures suggests lone-pair delocalization, hindered rotation, and thus an absence of protonation at the amino group. Second, the calculational results suggest that N-protonation is unlikely (vida infra).

Protonation of **3** at the β-carbon is ruled out by the peak patterns observed in both the 1D and 2D NMR spectra. β-Carbon protonation results in rehybridization of the β-carbon to sp^3 and renders the $C_\alpha-C_\beta$ bond a single bond with essentially free rotation. Thus, the *N*-methyl proton region of the NMR spectrum should yield a single pair of peaks arising from the two distinguishable proton environments for the *N*-methyl groups (Scheme 2). This is *not* consistent with the three peaks seen in Figures 1 and 2.

The likely site of protonation of **3** is the cyano nitrogen with formation of a ketenimine amidinium ion **9**. Protonation of the cyano group is consistent with the NMR spectral results. In **9** (X = NO_2), there are four distinguishable *N*-methyl proton

Table 2. Bond Lengths and Angles from B3LYP/6-31G*+p Calculations[a]

system	R(C═C)	R(C−N) (av)	R(C−C$_\phi$)	R(C−CN)	R(CN)	R(XH$^+$)	∠CNH$^+$	R(C−Y)
3								
unprotonated	1.404	1.376	1.470	1.424	1.168			1.460
CNH$^+$	1.465	1.348	1.491	1.346	1.204	1.019	125.8	1.478
CH$^+$	1.545	1.336	1.534	1.472	1.160	1.094		1.480
4								
unprotonated	1.400	1.379	1.477	1.424	1.168			1.500
CNH$^+$	1.464	1.348	1.493	1.345	1.205	1.019	125.3	1.510
CH$^+$	1.544	1.336	1.533	1.472	1.160	1.093		1.512
6								
unprotonated	1.395	1.382	1.482	1.423	1.168			1.352
CNH$^+$	1.462	1.349	1.493	1.345	1.206	1.019	124.9	1.338
CH$^+$	1.545	1.337	1.532	1.472	1.160	1.093		1.337
7								
unprotonated	1.394	1.383	1.482	1.424	1.168			1.511
CNH$^+$	1.461	1.349	1.493	1.345	1.206	1.019	124.6	1.509
CH$^+$	1.544	1.337	1.532	1.472	1.160	1.093		1.509

[a] Bond lengths in angstroms; angles in deg. X represents the atom to which the H$^+$ is attached, and Y represents the atom of the para substituent.

Table 3. Group Charges and Electric Dipole Moments for Unprotonated Systems from B3LYP/6-31G*+p

system	μ(D)	donor (e)	acceptor (e)	phenyl-X (e)
3	9.95	0.40	−0.40	−0.06
4	7.65	0.37	−0.37	−0.02
6	6.58	0.34	−0.34	0.01
7	6.16	0.33	−0.33	0.02

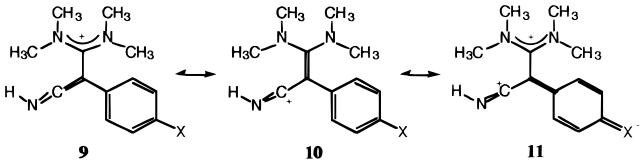

9 **10** **11**

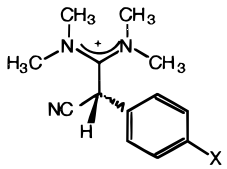

12

environments owing to the contribution of a resonance structure such as **10** (X = NO_2) where there is hindered rotation about the C═C bond. Exclusive CN-protonation by TFA and ketenimine formation in **3** occurs in all solvents studied, ranging in dielectric constant from $\epsilon = 5$ (chloroform) to $\epsilon = 20.9$ (acetone).

The temperature dependence of the aromatic signals in the NMR spectrum of protonated **3** also lends evidence for CN-protonation. Conjugation of the ketenimine with the aromatic ring is possible via resonance structure **11**. The partial double bond in the C−C(phenyl) bond contributes to hindered rotation of the aromatic ring and this process slows with decreasing temperature. This is manifested in the 1D NMR spectrum as a continual broadening of the signals from the aromatic hydrogens and in the 2D EXSY as exchange cross-peaks at very low temperatures (<−60 °C).

In compound **6**, the NMR spectra are a bit more complex. Addition of the even the smallest amount of TFA (0.25 equiv) results in six peaks in the *N*-methyl proton region. At 1.0 (or greater) equiv of TFA, the ratio of the higher intensity upfield peaks (4 peaks) to the lower intensity downfield peaks (2 peaks) is 87:13. The 2D EXSY spectrum is extremely useful in sorting out the various species and dynamics in this sample. We attribute the low-temperature spectral pattern and 2D EXSY cross-peak pattern to the existence of both a C$_\beta$-protonated form of **6** (**12** (X = F)) and a CN-protonated (ketenimine, **9** (X = F)) form, in a ratio of 13:87. The two smaller peaks in this *N*-methyl proton region result from the C$_\beta$-protonated tautomer. In **12** (X = F) there is relatively free rotation about the C$_\alpha$−C$_\beta$ bond, distinguishing only two *N*-methyl groups that are interchanged via C−N bond rotation. This rotation leads to the cross-peak between the two diagonal peaks of the C$_\beta$-protonated form in the 2D EXSY. The four upfield peaks correspond to the *N*-methyl groups of the ketenimine amidinium ion, **9** (X = F), similar to protonated **3**. The cross-peaks among these four peaks arise due to the dynamic processes diagrammed in Scheme 2 (for the unprotonated compound). The cross-peaks connecting the peaks from **12** (X = F) with those from **9** (X = F) correspond to intermolecular exchange of the two forms, via proton transfer. The absence of any broadening of the aromatic signals corresponding to the C$_\beta$-protonated forms of **4**−**7** are consistent with the sp^3 hybridization of C$_\beta$.

Additional evidence for the two protonated forms of **6** are given by the two sets of peaks in the aromatic region of the NMR spectrum. The 2D EXSY shows cross-peaks between diagonal peaks, again indicating intermolecular exchange via proton transfer between the two protonated forms (as monitored by the aromatic protons).

The situation in enamine **7** under acidic conditions is quite similar to that in **6**. The familiar six-peak pattern in the *N*-methyl proton region of the low-temperature NMR spectrum of **7** in the presence of TFA is observed in $CDCl_3$, CD_2Cl_2, or $CD_3C(O)CD_3$. Intermolecular exchange via proton transfer between the two protonated forms as well as intramolecular exchange via bond rotations are again obvious from the cross-peak patterns in the 2D EXSY of **7** (not shown). Enamine **7**, however, shows a ratio of CN-protonated to C$_\beta$-protonated tautomers of 60:40. Again, formation of the ketenimine amidinium ion **9** (X = CH_3) is preferred relative to the amidinium ion **12** (X = CH_3) in this push−pull system.

The calculations yield both structural and energetic data that is in agreement with the experimental data. Table 1 clearly shows that in all cases the result of protonation on the amino nitrogen leads to a structure which lies at least 15 kcal mol^{-1} higher in energy than the C$_\beta$- or CN-protonated forms. The size of this energy difference is well outside the error bounds one would expect from calculations of this type. When coupled with the experimental evidence, the calculations argue convincingly that protonation of the amino nitrogen is not favorable.

Distinguishing protonation at the β-carbon versus the cyano nitrogen is less obvious from the calculations since the energy

differences are quite small. Table 1 shows that in all cases the calculations predict that the CN-protonated enamine lies lower in energy than the C_β-protonated form. The calculated CN-protonated/C_β-protonated energy differences follow the order **3** > **4** > **6** > **7** with or without the addition of ZPE corrections. No claims are made that the current calculations are able to obtain accuracies of a few tenths of a kcal mol^{-1}; however, the experimental and calculational results strongly support the interpretation of CN-protonation over C_β-protonation. The fact that calculations performed with a number of basis sets give such consistent results also strongly supports their integrity.

The structural changes implied by the NMR spectra are also borne out in the calculations. Perhaps the most telling aspect of the structural changes indicating formation of a ketenimine is the decrease of the C−CN bond length upon CN-protonation (Table 2). This decrease is almost 0.08 Å and results in a C−CN bond comparable in length to what one would expect for a true C═C double bond. Consistent with this is the smaller increase in the cyano CN bond which amounts to nearly 0.04 Å and the C−N−H angle in the CN-protonated species which is 125°. An angle of this size certainly implies an sp^2 hybridized nitrogen atom as opposed to a 180° angle that would indicate sp hybridization.

In all C_β- or CN-protonated species, the C═C bond length increases dramatically from that in the unprotonated molecule. There is an increase of 0.06−0.07 Å for CN-protonation, but an even larger increase of 0.14−0.15 Å occurs for C_β-protonation. The resultant bond lengths in the case of C_β-protonation are in line with what one would expect for a C−C single bond. Furthermore, after C_β-protonation the gross structure around this carbon is tetrahedral. Both of these results are once again consistent with a small energy barrier for C−C rotation. Protonation on either the β-carbon or the cyano nitrogen has a pronounced effect on the C_α−N bonds of the amine groups. These bonds show decreases of 0.03 Å (CN-protonation) and 0.04−0.05 Å (C_β-protonation) which imply a higher barrier for C_α−N rotation. Significant changes are also seen in the C_β−C(phenyl) bond lengths. This length increases by 0.05−0.06 Å for the C_β-protonation and about one-half this value for CN-protonation. The shortening of this bond upon CN-protonation is also consistent with the experimental evidence of restricted rotation of the phenyl group.

It is interesting to note that the predicted C_α−C_β "double" bond lengths in the unprotonated systems are all calculated to be longer than the C_α−N "single" bond lengths. This is consistent with the highly delocalized π-electron systems in these molecules which leads to their low C_α−C_β and high C_α−N rotational barriers in the unprotonated forms.

The steric crowding of the bis(*N*,*N*-dimethylamino) moiety with the phenyl ring in **3**−**7** leads to nonplanarity about the C═C in the unprotonated push−pull molecules. Indeed, the dihedral angle about the C═C (between the N−C_α−N plane and C(cyano)−C_β−C(phenyl) plane) is around 30° in unprotonated **3**−**7**. This precludes optimum overlap of the lone pair electrons on the nitrogens with the parallel p orbitals of the C═C. However, the conjugation and delocalization of these electrons throughout the π system is evident from the variations in C═C and C−N rotational barriers measured by Kessler.[7] Protonation of **4**−**7** at C_β completely disrupts the conjugation between the two "halves" of the molecule, and the phenyl ring twists 20° further to decrease steric crowding. On protonation of **3**−**7** at the cyano nitrogen, the dihedral angle about the C═C increases to 40° while the phenyl ring twists an additional 10° relative to the unprotonated molecule, forcing it further from planarity. These dramatic structural changes that occur on protonation make it unlikely that the substituted phenyl ring is able to interact with the positive charge developing in the protonated amidinium ion.

Although the protonation energy differences between C_β and CN are largest in **3**, this system shows the smallest PAs. In fact, the CN-protonation energy in **3** is calculated to be 10 kcal mol^{-1} less than that for **7**. The explanation for this may lie in the strong electron-withdrawing ability of the $-NO_2$ group which gives the phenyl ring a slightly more negative overall charge than in **7**. Similar arguments hold when comparing the PAs for the other systems. Even though the total negative charge on the acceptor portion of the molecule is the largest in **3**, the delocalization of electron density onto the phenyl ring comes largely at the expense of C_β. This makes the CN site more electron rich in comparison with C_β. These results are in agreement with the moderately large, positive ρ value derived from the Hammett-type relationship shown in Figure 6.

The fact that the calculations did not include solvent effects will certainly change the relative energy differences C_β- versus CN-protonated enamines. However, the calculations clearly indicate that protonation of the cyano nitrogen is competitive with protonation of the β-carbon. In addition, the energy differences between CN- and C_β-protonated forms (**3** > **4** > **6** > **7**) should be relatively independent of solvent due to the structural similarities. Another inadequacy of the theoretically calculated energy differences is that they do not include thermal effects, but correspond to the energy differences at T = 0 K. Estimates of the thermal effects for the in vacuo systems, as calculated from the Gaussian 94 program using the B3LYP/6-31G calculations indicate that these effects are small (∼0.1 kcal mol^{-1}).

To probe the effect of solvent on the relative stabilities of the CN-protonated and C_β-protonated systems more closely, the equilibrium distribution data was analyzed for **6** and **7**. For **4** and **5** the small amount of C_β-protonated enamine relative to CN-protonated enamine renders the integration less certain and were not analyzed. Plots of ln K_{eq} vs T^{-1} (not shown) for the process:

$$C_\beta\text{-protonated} \rightleftharpoons \text{CN-protonated}$$

were made over the temperature ranges 0 to −50 °C (5 points) and −20 to −60 °C (4 points). In both cases the results were extremely linear ($R^2 = 0.99$). The $\Delta H°$ and $\Delta S°$ values extracted from these fits are 2.5 kcal mol^{-1} and 15 cal K^{-1} mol^{-1} for **6** and 1.9 kcal mol^{-1} and 11 cal K^{-1} mol^{-1} for **7**. Interestingly, the $\Delta H°$ values for the proton transfer are positive. If the calculated in vacuo results for the relative stabilities are taken as reasonable estimates of the in vacuo $\Delta H°$ values, this means that solvation stabilizes the C_β-protonated form more than the CN-protonated enamine. Due to the small $\Delta H°$ term, the position of the equilibrium is determined by the positive $\Delta S°$ term. Estimates of $\Delta S°$ from the calculations reveal that this difference is small for the isolated molecules (<1 cal K^{-1} mol^{-1}). Once again, this implies that the major difference in the $\Delta S°$ term arises from the solvent effect.

The altered reactivity toward acid observed in the β-cyano-enamines **3**−**7** studied here is analogous to that seen in the synthetically useful enaminones (push−pull enamines with (−C(═O)R as electron-withdrawing group). Delocalization of electrons into the carbonyl group facilitates protonation on oxygen[26] in nearly all cases of enaminones and enaminoesters.

(26) (a) Kozerski, L.; Dabrowski, J. *Org. Magn. Reson.* **1972**, *4*, 253. (b) Berg, U.; Sjostrand, U. *Org. Magn. Reson.* **1978**, *11*, 555.

Conclusion

The experimental NMR and quantum mechanical results reported here present convincing evidence that the favored site of protonation in the β-cyanoenamines **3**−**7** is the cyano group. This results in the formation of a ketenimine in solution and is manifested in the 1D and 2D NMR experiments. The NMR data indicate 100% CN-protonation in **3**, 93% in **4** and **5**, 87% in **6**, and 60% in **7**. The experimental energy difference between the CN-protonated and C_β-protonated forms is small enough in **4**−**7** that equilibrium mixtures are observed; however, in all cases the ketenimine is preferred. Calculational results support the cyano group as the site of protonation and reproduce the small difference in the protonation energies of the two sites. Calculated structures give further evidence that a ketenimine is formed as implied by the extremely short C_β−CN and elongated cyano CN bond length upon CN-protonation.

Acknowledgment. This work was supported in part by Petroleum Research Fund Grant 26794-GB4 (T.J.D.). The Varian UNITY300 NMR was acquired through an NSF-ILI grant (DUE9051310).

JA983016M